



This is a repository copy of *The influence of ultrasonic surface rolling on the fatigue and wear properties of 23-8N engine valve steel*.

White Rose Research Online URL for this paper:
<http://eprints.whiterose.ac.uk/144750/>

Version: Accepted Version

Article:

Lai, F., Qu, S., Lewis, R. et al. (3 more authors) (2019) The influence of ultrasonic surface rolling on the fatigue and wear properties of 23-8N engine valve steel. *International Journal of Fatigue*. ISSN 0142-1123

<https://doi.org/10.1016/j.ijfatigue.2019.04.010>

© 2019 Elsevier. This is an author-produced version of a paper subsequently published in *International Journal of Fatigue*. Uploaded in accordance with the publisher's self-archiving policy. Article available under the terms of the CC-BY-NC-ND licence (<https://creativecommons.org/licenses/by-nc-nd/4.0/>)

Reuse

This article is distributed under the terms of the Creative Commons Attribution-NonCommercial-NoDerivs (CC BY-NC-ND) licence. This licence only allows you to download this work and share it with others as long as you credit the authors, but you can't change the article in any way or use it commercially. More information and the full terms of the licence here: <https://creativecommons.org/licenses/>

Takedown

If you consider content in White Rose Research Online to be in breach of UK law, please notify us by emailing eprints@whiterose.ac.uk including the URL of the record and the reason for the withdrawal request.



eprints@whiterose.ac.uk
<https://eprints.whiterose.ac.uk/>

Accepted Manuscript

The influence of ultrasonic surface rolling on the fatigue and wear properties of 23-8N engine valve steel

Fuqiang Lai, Shengguan Qu, Roger Lewis, Tom Slatter, Wenlan Fu, Xiaoqiang Li

PII: S0142-1123(19)30134-3

DOI: <https://doi.org/10.1016/j.ijfatigue.2019.04.010>

Reference: JIJF 5072

To appear in: *International Journal of Fatigue*

Received Date: 6 November 2018

Revised Date: 3 April 2019

Accepted Date: 7 April 2019

Please cite this article as: Lai, F., Qu, S., Lewis, R., Slatter, T., Fu, W., Li, X., The influence of ultrasonic surface rolling on the fatigue and wear properties of 23-8N engine valve steel, *International Journal of Fatigue* (2019), doi: <https://doi.org/10.1016/j.ijfatigue.2019.04.010>

This is a PDF file of an unedited manuscript that has been accepted for publication. As a service to our customers we are providing this early version of the manuscript. The manuscript will undergo copyediting, typesetting, and review of the resulting proof before it is published in its final form. Please note that during the production process errors may be discovered which could affect the content, and all legal disclaimers that apply to the journal pertain.



The influence of ultrasonic surface rolling on the fatigue and wear properties of 23-8N engine valve steel

Fuqiang Lai^{1,2}, Shengguan Qu^{1*}, Roger Lewis², Tom Slatter², Wenlan Fu³, Xiaoqiang Li¹

1. Guangdong Key Laboratory for Advanced Metallic Materials Processing, School of Mechanical and Automotive Engineering, South China University of Technology, Guangzhou 510640, Guangdong, China

2. Department of Mechanical Engineering, The University of Sheffield, Mappin Street, Sheffield, UK, S1 3JD

3 Huaiji Dengyun Auto-parts (Holding) CO., LTD. Huaiji County 526400, Guangdong, China

Abstract:

An ultrasonic surface rolling (USR) technique was employed for the first time as a method to enhance the fatigue and wear resistance of 33Cr23Ni8Mn3N (23-8N) austenitic engine valve steel. The microstructure of the modified layer on the material surface was characterised by scanning electron microscopy (SEM) coupled with electron back scatter diffraction (EBSD) and transmission electron microscope (TEM) methods. Nanoscale lamellar grains were discovered on the top surface of the treated material, and an increase of compressive residual stress and microhardness of the surface material observed. A comparative fretting wear test and a rotating bending fatigue test were performed out to verify the surface enhancement effect. Fractured and worn faces of specimens were evaluated through utilizing SEM and energy-dispersive spectroscopy (EDS). Compared to the untreated material, the coefficient of friction of USR treated material was significantly reduced, and the wear resistance was improved. The fatigue strength of a specimen treated at 25 °C was increased from 528 MPa to 730 MPa (38.3 %). At 650 °C, the fatigue strength increased from 345 MPa to 400 MPa (15.9 %). The fatigue resistance extension and wear resistance improvement of

Corresponding Author * : Shengguan Qu, Professor; E-mail: qusg@scut.edu.cn. Tel: +86-020-87111983.

treated specimen can be attributed to a combination of beneficial compressive residual stress, work hardening, and the modified microstructure with fine-grains in the surface layer, and thus demonstrates the validity of this novel technique.

Key words: ultrasonic surface rolling; surface enhancement; engine valve steel; fatigue properties; wear properties

List of abbreviations and symbols

USR	Ultrasonic surface rolling	EBSD	Electron back scatter diffraction
GD	Grain diameter	EDS	Energy–dispersive spectroscopy
KAM	Kernel average misorientation	SEM	Scanning electron microscopy
CoF	Coefficient of friction	TEM	Transmission electron microscope

1. Introduction

The operating conditions and environment of internal combustion engine exhaust valves are extremely severe. The exhaust valves must resist high frequency cyclic stress generated from the valve motion and combustion pressure, high temperature and corrosive environments, and the possible presence of particulates and third bodies [1, 2]. The recent increases in specific performance of internal combustion engines has resulted in an increase of combustion chamber temperature and particularly pressure. In addition, due to the washout of the exhaust gas, the concave area of exhaust valve suffers notably high temperatures. For instance, the temperature distributions of a traditional solid exhaust valve were measured in previous research [3], as presented in Fig 1(a) where the results were obtained via a thermometric valve installed in a dynamometer gasoline engine. It was found that the temperature of the concave area of an exhaust

valve was at a comparatively high level.

Similarly, the concave area of the valve withstands much higher stress, as indicated by the white circle in Fig 1(b). The stress contours were obtained from simulation results of exhaust valves using a finite element method. It is also reported by Worthen and Rauhen that the concave area of an engine valve is at a high stress level [4]. Furthermore, the improper assembly of the valve and seat insert and heat deformation of the cylinder head might cause a distortion of the seat insert in a firing engine. Subsequently, the distortion would lead to bending loads acting on the concave area of valves [5]. Failure is most likely to occur near the concave area of the valve and would be catastrophic to the engine once the valve head is fractured. Consequently, surface enhancement treatments are increasingly required to be applied to internal combustion engine exhaust valve designs, improving fatigue resistance at high temperatures.

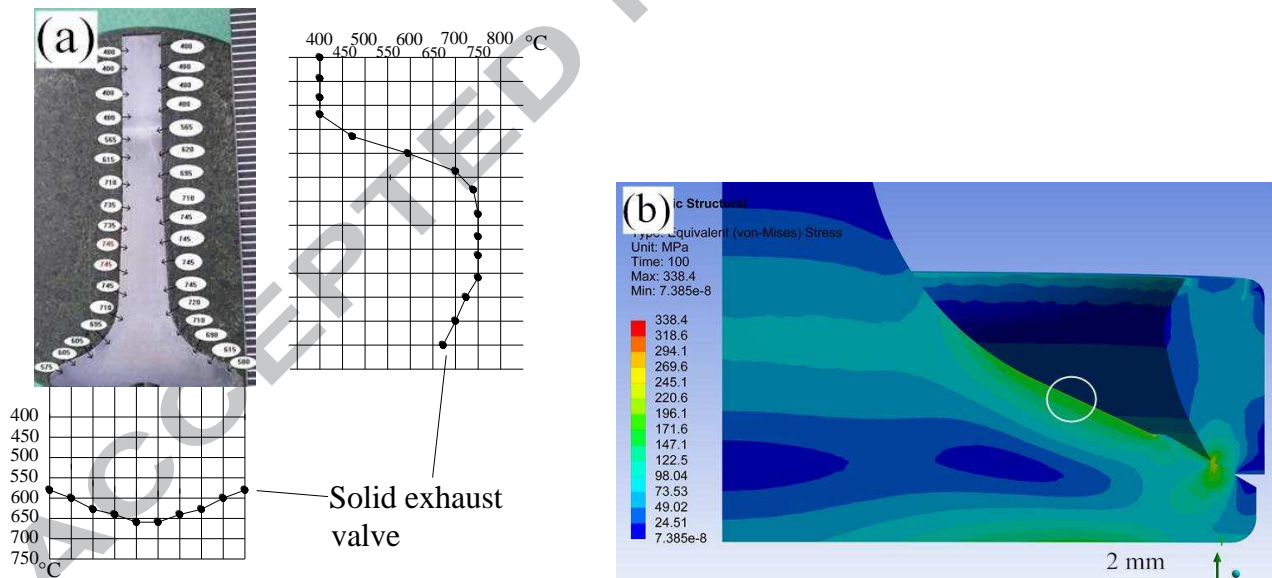


Fig. 1. (a) Exhaust valve operating temperature [3]; (b) finite element method results of valve head stress contours with combustion pressure.

Nitriding treatment is a common surface enhancement technology for engine valves, leading to superior wear resistance and suitable structure performance [6]. Shot peening can improve the

fatigue strength of spring steel and tempered martensitic steel [7, 8], and it is reported by Nalla et al. that the fatigue strength of Ti-6Al-4V at ambient and elevated temperatures was significantly increased after deep rolling and laser shock peening treatment [9]. Surface enhancement treatments combined with ultrasonic technology have been developed in recent decades. Ultrasonic nanocrystal surface modification has been applied to the plasma-nitrited S45C steel [10], quenching and tempering S45C steel [11], 40Cr steel [12], Inconel 690 alloy [13], as well as normal and heat-treated 60kgK rail steel [14]. During the ultrasonic nanocrystal surface modification processes, the material surface is struck as force was applied by a hard ball up to tens of thousands of times per second, leading to a severe plastic deformation in the surface and subsurface of materials. These strikes can be considered as having a micro-cold-forging process [14]. Similarly, ultrasonic surface rolling (USR) also has been applied to in a titanium alloy in previous work of Qu et al. [15-17]. During the USR processing, a hard ball not only struck the surface of materials at the high frequency of ultrasonic vibration, but also rolled on the surface of materials. The fretting wear resistance and fatigue strength of titanium alloy were clearly increased after USR treatment.

Although surface enhancement treatments with ultrasonic technology has been developed for many components and types of materials, little research on engine valve components and materials can be found in the published literature. In the work presented here, USR treatment was applied to an engine valve steel. Details of the USR processing are presented, together with the resulting surface microstructure characterized by scanning electron microscopy (SEM) coupled with electron back scatter diffraction (EBSD) and transmission electron microscope (TEM). The surface properties include residual stress, micro-hardness, surface roughness were evaluated, and the surface enhancement effect was verified by comparative rotating bending fatigue test and comparative

fretting wear test in dry conditions. After the fatigue and fretting wear test, the fractured and worn faces of specimens were characterized using SEM and energy-dispersive spectroscopy (EDS). The fatigue mechanisms and wear mechanisms are also discussed.

2. Experimental details

2.1 Materials

The material selected for use in this work, 33Cr23Ni8Mn3N (23–8N) austenitic steel is commonly used for exhaust valves in modern internal combustion engines. The steel bar was provided by a commercial steel manufacturer with solution annealing status, following the Chinese Standard of GB/T 23337–2009 (Internal combustion engines – Intake and exhaust valves – Specification). Subsequently, the steel had a full ageing heat treatment applied (aged at 800 °C for 16 h, consequently cooled down to room temperature in the air). The chemical composition of the 23–8N steel is presented in Table 1. The steel hardness at room temperature was 31.2 ± 0.6 HRC and the selected mechanical properties of the steel are presented in Table 2.

Table 1 Compositions of 23–8N steel specimens (wt. /%).

	C	Si	Mn	P	S	Ni	Cr	N	Mo	Fe
GB/T 23337–2009	0.28~ 0.38	0.50~ 1.00	1.50~ 3.50	≤ 0.040	≤ 0.030	7.00~ 9.00	22.00~ 24.00	0.25~ 0.35	≤ 0.05	Bal.
Specimens	0.32	0.81	2.01	0.028	0.007	7.15	22.45	0.31	0.001	Bal.

Table 2 Mechanical properties of 23–8N steel.

Temperature, T (°C)	Tensile strength, σ_b (MPa)	Yield strength, σ_s (MPa)	Elastic modulus, E (GPa)
------------------------	---------------------------------------	-------------------------------------	-----------------------------

25	1002	605	183
650	579	310	149

2.2 USR treatment

After the heat treatment, the steel bars were machined into smaller bars and hourglass shape specimens. They were then processed by USR on a lathe using a tungsten carbide rolling ball. Based on the methodology presented in the previous investigations of Qu et al. on titanium alloy with hardness of 325 HV [15-17], the residual stress and hardened depth of modified layer was increased when the static force was increased from 600 N to 900 N. Hence, optimized processing parameters of USR were chosen and they are listed in Table 3. The applied static force was chosen at 900 N and the amplitude of vibration was set at 10 μm . The frequency of ultrasonic vibration was respectively chosen at 20 kHz and 30 kHz, and an air compressor was used to support the static force at a certain air pressure. A schematic and photographic images of the USR treatment are presented in Fig. 2(a) and (b), and of the hourglass shape specimens used for the fatigue test after treatment are presented in Fig. 2(c). The rolling ball vibrated and rolled against the surface of materials during the processing, and was lubricated and cooled by environmental Inner HM 111 rapeseed oil base cutting compound, in order to avoid high temperatures on the specimen surface.

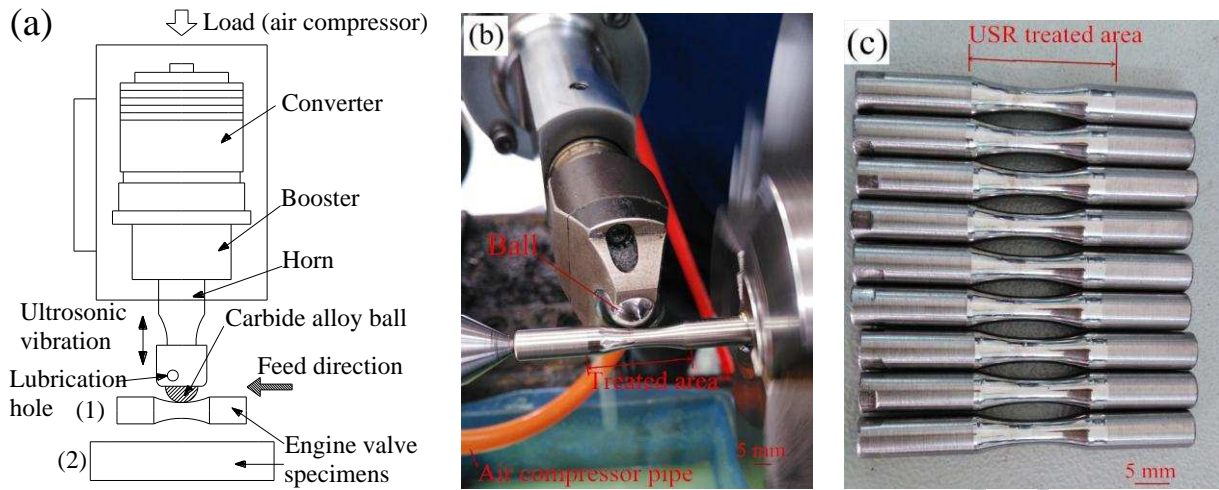


Fig. 2. (a) Schematic of USR treatment; (b) USR treatment; (c) specimens after USR treatment.

Table 3 USR processing parameters.

Frequency	Ball diameter	Load	Amplitude	Spindle speed	Axial feed
(kHz)	(mm)	(N)	(μm)	(rpm)	(mm/rev)
20, 30	15	900	10	45	0.08

2.3 Microstructure analysis

The cross-sectional microstructure was polished by ion etching then characterized by EBSD (Hitachi S-3400 N SEM equipped with an HKL-EBSD system, Japan). The surface of the materials after USR treatment was processed using a focused ion beam method to prepare specimens for TEM (TECNAIG2S, FEI, USA). TEM images and the corresponding selected area electron diffraction were obtained by TEM, and the accelerating voltage was set at 200 kV. The evolution of microhardness of cross-sectional was evaluated by a Vickers microhardness tester (MVS 1000D1, Guangjing, China). During the microhardness tests, the load was applied by a 0.2 kg mass and dwelling time was 15 s. The residual stress results were obtained by a x-ray diffraction method

(LXRD, Proto, Canada).

2.4 Fretting wear test

The specimens for fretting wear tests were taken from bars with and without USR treatment applied. The wear tests were performed using a ball-on-disk fretting tribometer (SRV IV, Optimol, Germany). A photograph and schematic diagram of the tribometer are presented in Fig. 3(a) and (b), respectively. Based on the experience of previous friction and wear research on a titanium alloy with and without USR treatment [15], similar test parameters were chosen and they are listed in Table 4. The load was set at 5 N in the run-in period with the first 5 minutes for every specimen, then the load was set at different levels in the later 30 minute test period for the corresponding specimen. The oscillation frequency was set at 10 Hz, which equals 18,000 reciprocating sliding cycles in each test period. The other parameters such as oscillation frequency and stroke were kept the same with all specimens. The same test parameters were used for the untreated and treated materials to obtain data for the wear resistance comparison and evaluation. All the tests were carried out without lubrication at room temperature in the ambient atmosphere (25 °C, humidity of 70 %). The counterface was a Si_3N_4 ceramics ball with a diameter of 10 mm for each test.

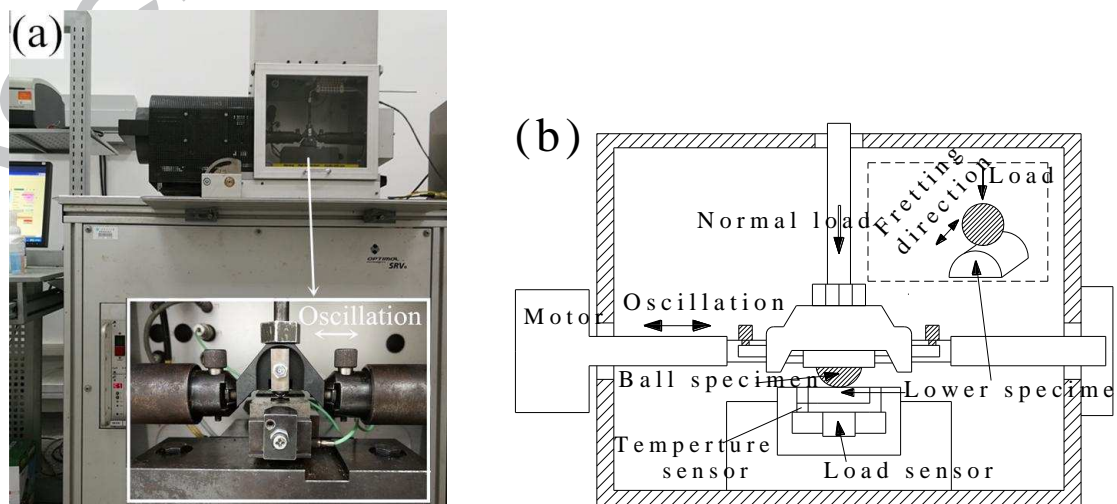


Fig. 3 Ball-on-disk fretting tribometer: (a) photograph with cutaway detail; (b) schematic diagram.

Table 4 Fretting wear test parameters.

Run-in period load (N)	Run-in period time (min)	Test period load (N)	Test period time (min)	Frequency (Hz)	Stroke (μm)
5	5	5, 10, 20, 40	30	10	200

2.5 Fatigue test

In order to improve the performance and durability life of engine valves, USR treatment can be applied in the concave area of the engine valve components during the manufacturing process. However, such comparative fatigue tests of engine valve components should ideally be conducted in a firing dynamometer engine or a specially designed apparatus, and this can be very resource intensive. Thus, the pilot study fatigue test was carried out through a rotating bending fatigue tester (QBWP, Changchun, China) utilizing material specimens, and the schematic diagram of the tester is presented in Fig. 4(a). The rotating bending fatigue test was performed with a stress ratio of $R = S_{\max} / S_{\min} = -1$, and a frequency of 100 Hz. For instance, the waveform of stress at a position on the central surface of hourglass shape specimen is presented in Fig. 4(b). The fatigue specimens were tested at two temperatures (25°C and 650 °C) in the ambient atmosphere and after ten million cycles had occurred the fatigue testing was automatically suspended. It should be noted that the small material fatigue specimens with hourglass shape were used in the rotating bending fatigue tester. Bending stress amplitude σ in the net section of the specimen was estimated by accounting for the balance of the inertia forces arisen at bending load, as presented in Equation (1) [18].

$$\sigma = \frac{M \cdot y}{I} \quad (1)$$

where σ is the bending stress, M is the bending moment, y is the distance from the neutral axis, and I is the moment of inertia of the cross section.

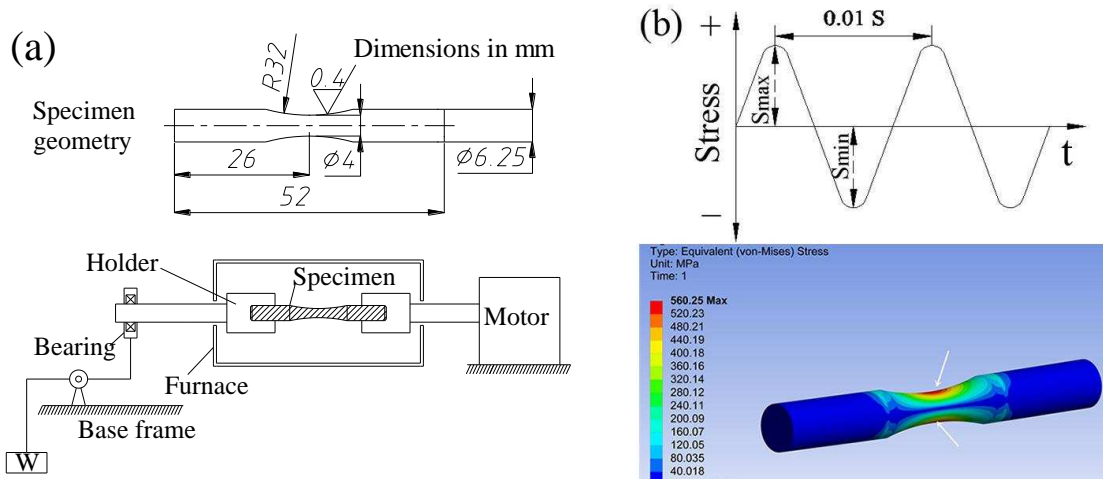


Fig. 4 (a) Schematic diagram of rotating bending fatigue tester and specimen geometry;

(b) the waveform of stress at a position on the central surface of hourglass shape specimen.

3. Results and discussion

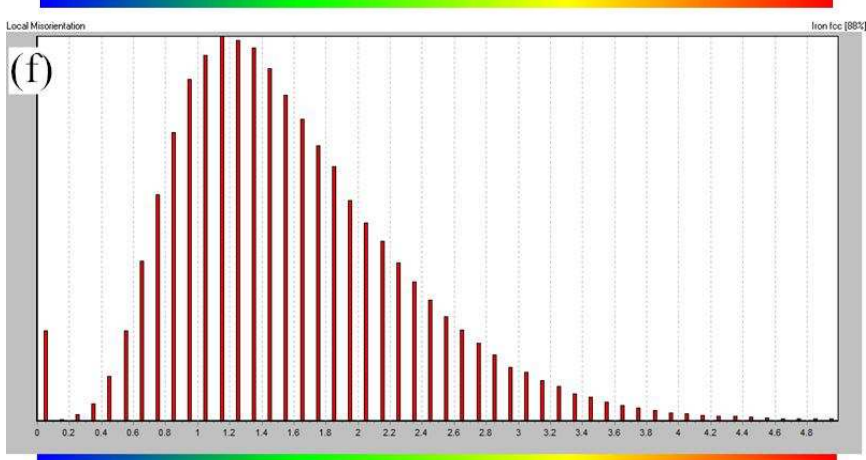
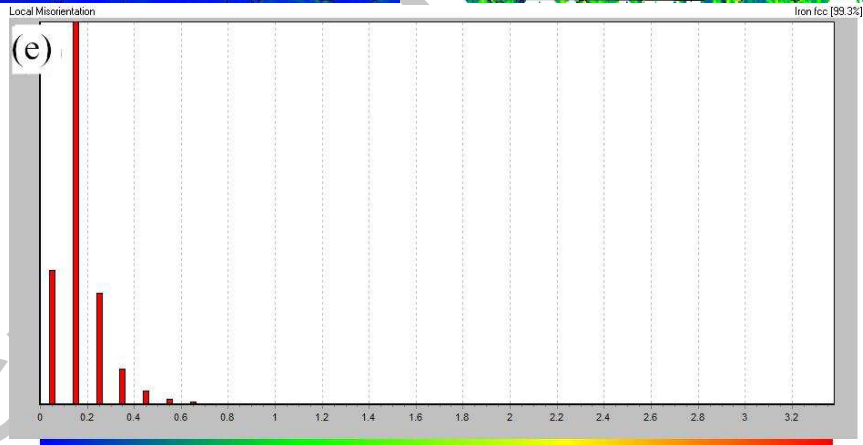
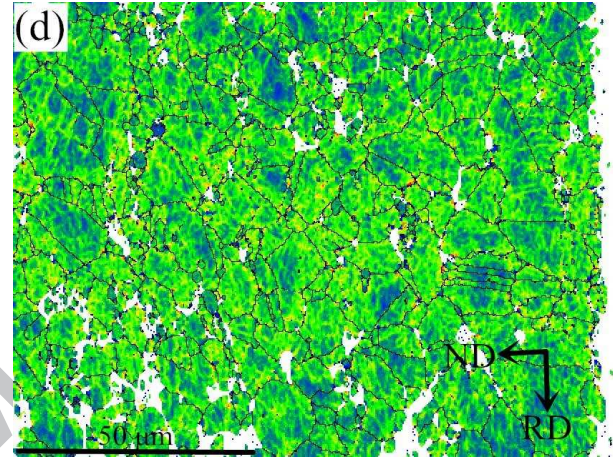
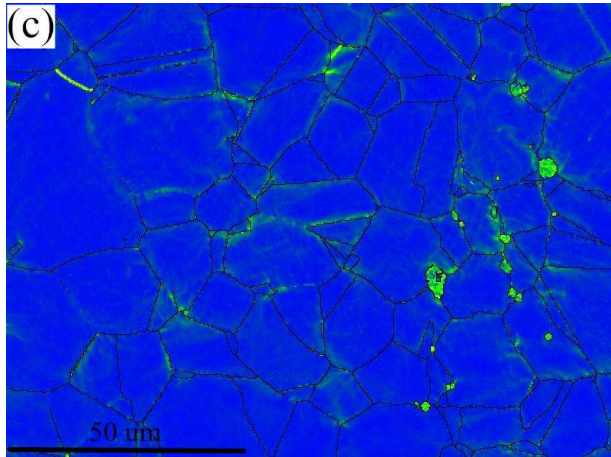
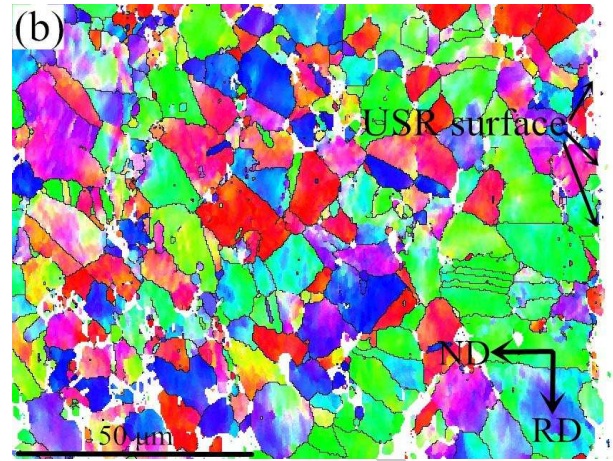
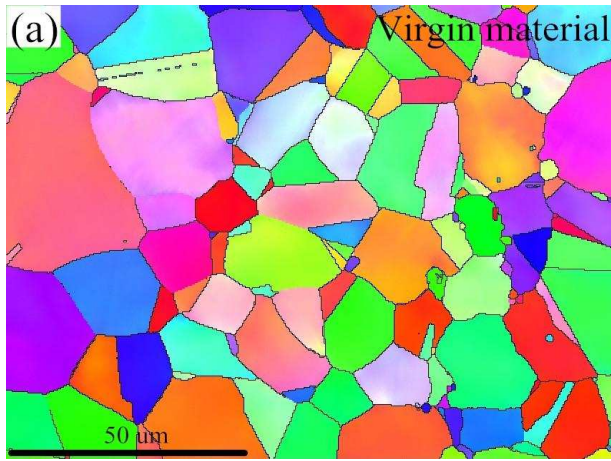
3.1 Microstructure

The results of cross-sectional EBSD observations of the as-received virgin (i.e. not treated with USR) material and USR treated (30 kHz, 900 N) material are presented in Fig. 5-7. The crystal orientation map of the two materials is presented in Fig. 5(a) and (b), where RD represents the rolling direction (feed direction of the rolling ball) and ND represents the normal direction. Kernel average misorientation (KAM) during EBSD analysis can be used as a measure of local grain misorientation and the average misorientation around a measurement point with respect to a defined set of nearest neighbour points is quantified in KAM [19]. The KAM distribution of the untreated and treated material is presented in Fig. 5(c) and (d). The blue colour indicates the smaller

misorientations of grains, the larger misorientations are shown in yellow and red colour. The KAM curves of the two materials are presented in Fig. 5(e) and (f), respectively. Based on the results presented in Fig. 5(e) to (f), it is observed that the treated material had a higher value of KAM than the untreated material. As reported by Li et al. [20], generally KAM is high in deformed grains due to higher dislocation density. It can be inferred that the deformation and strain of the grains in the treated material was significantly increased.

The statistical results of grains are shown in Fig. 5(i). It is found that the average of grain diameter (GD) of the virgin material was 6.77 μm , the average area of grain was 149.48 μm^2 , and the GD of 53.1 % of the grains was lower than 1 μm and 23.1 % higher than 10 μm . The treated specimen was observed in a region close to the top surface, which is indicated in the right edge in Fig. 5(b). The average of GD of the USR treated material was 1.70 μm , the average area of grain was 13.51 μm^2 , and the GD of 73.5 % of grains was lower than 1 μm . However, only 3.8 % of the grains's GD was higher than 10 μm . It is determined that the grain refinement was evident after USR treatment at 30 kHz at 900 N.

The direction of any three-dimensional vector in a crystal, i.e. a crystallographic direction or the normal to a crystal plane, could be described as a point on the reference sphere. Pole is the point of intersection of normal to this figure [21]. Pole figure represents the orientation of the crystal coordinate system in the specimen coordinate. The pole figures of two materials are presented Fig. 5(g) and (h). It is found that the virgin material possessed weak textures, and the density of pole was comparatively high. However, the orientation of grains of the USR treated material were distributed more randomly, suggesting that the steel did not hold the texture after USR treatment and the density of pole was significantly decreased.



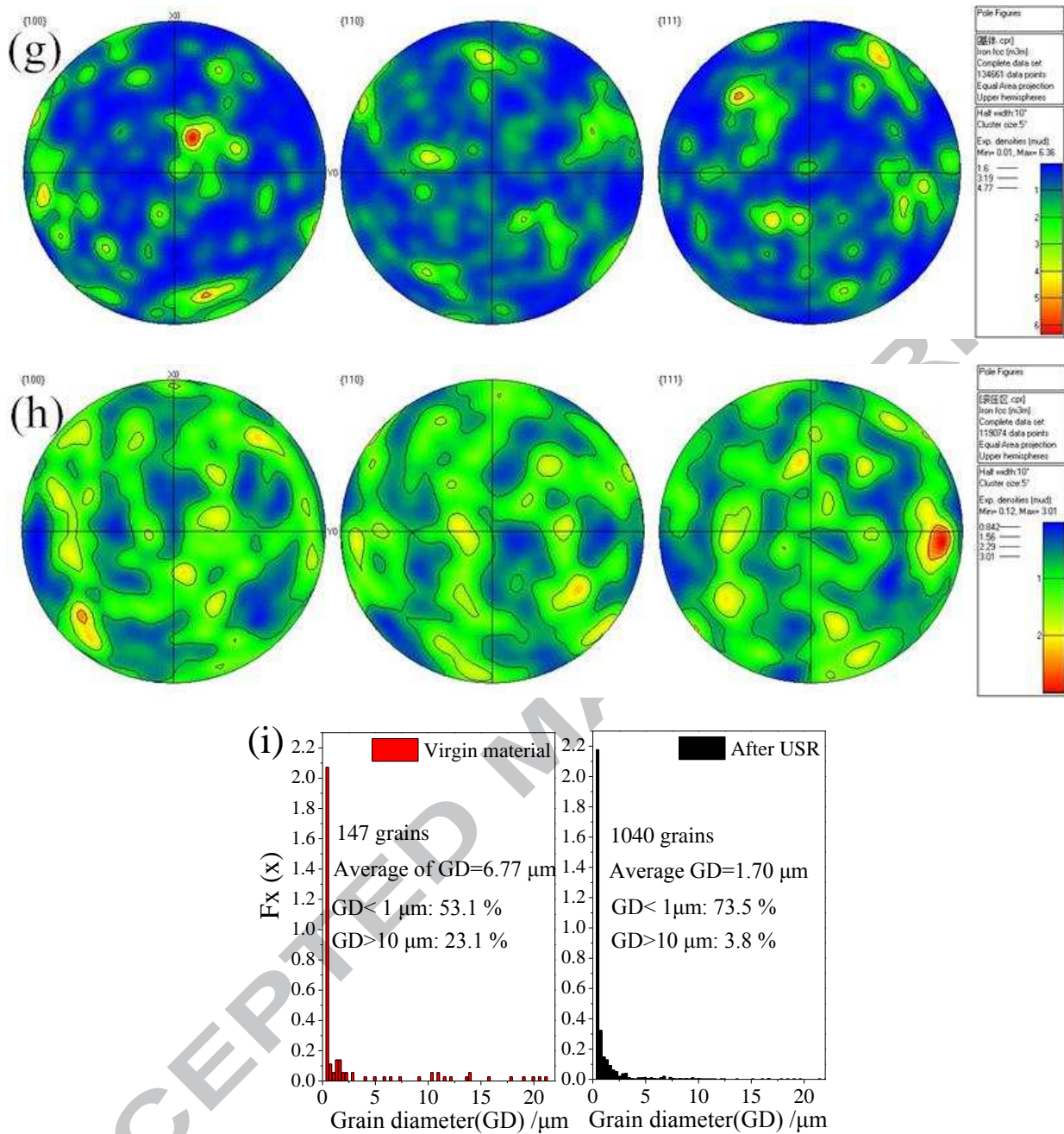


Fig. 5 (a) Crystal orientation map of the virgin material; (b) crystal orientation map of the USR treated material; (c) KAM distribution of the virgin material; (d) KAM distribution of the USR treated material; (e) KAM curve of the virgin material; (f) KAM curve of the USR treated material; (g) pole figure of the virgin material; (h) pole figure of the USR treated material. (i) statistical result of grains of two materials.

Fig. 6(a) and (b) presents the recrystallization map of two materials, and the statistical result of grain

recrystallization status is presented in Fig. 6(c). Compared to the virgin material, the proportion of recrystallized grains and substructured grains were decreased, however, the proportion of deformed grains was significantly increased. As reported by Wang et al., grain refinement in 40Cr steel during the ultrasonic surface rolling processing is mainly produced by deformation, and plastic deformation takes place primarily by dislocation movements [12]. Dislocations tangle with each other and then to form cellular structures which then develop to subgrains (with independent slip systems). With the increase of strain, subgrains turn to new grains with small or big angle grain boundaries [12]. It can be indicated that the deformed grains resulted from severe plastic deformation from the high frequency vibration and surface rolling. This also agrees well with the fact that the difference of recrystallization maps of virgin and USR treated material (Fig. 6(a) and (b)).

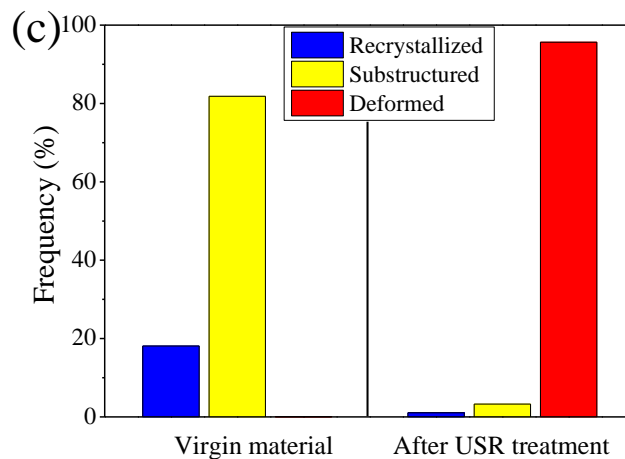
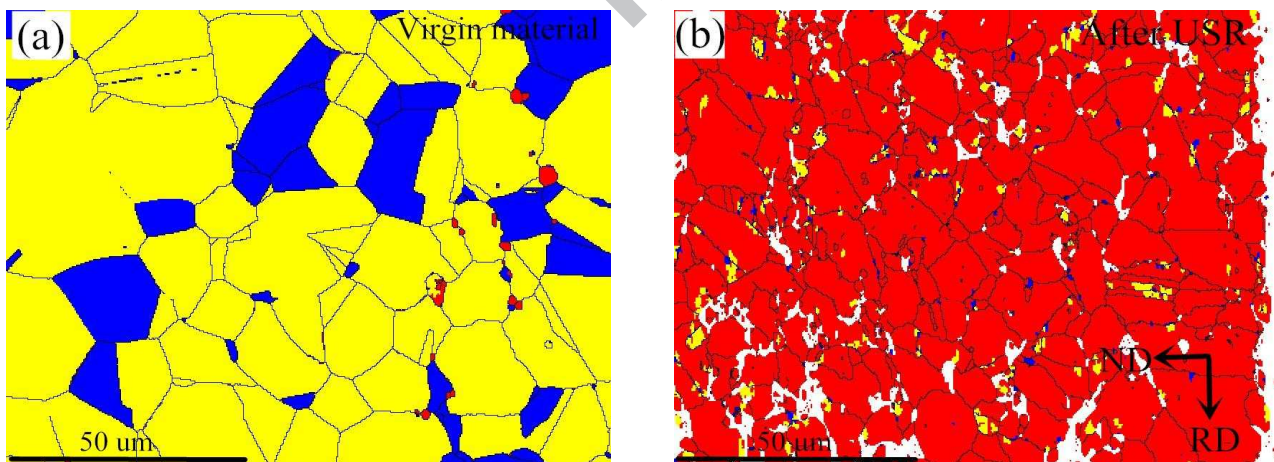


Fig. 6 (a) Recrystallization map of virgin material, (b) recrystallization map of USR treated material; (c) statistical result of recrystallization of two materials.

In order to obtain a better characterization of microstructure of the region near the top surface of the treated specimen, the severe plastic deformation layer was detected by focused ion beam and TEM analysis, and the corresponding selected area electron diffraction were obtained by TEM. A TEM image from the top surface of the USR treated (30 kHz 900 N) specimen is presented in Fig. 7(a). It is found that the microstructure consisted of nanoscale lamellar grains, some grain boundaries were marked with dotted lines and arrows in the figure. The width of the grains was about 50–150 nm. In addition, there are many rings in the corresponding selected area electron diffraction pattern (Fig. 7(b)), indicating the presence of nano-grains [13, 22]. Furthermore, the lamellar grains consisted of nanostructured subgrains, as presented in the enlarged image of grains (Fig. 7(c) and (d)). The subgrains had a non-uniform morphology, and the subgrains displayed blurred boundaries (Fig. 7(d)). As reported by Kheradmandfard et al. [22], similar results was found in β -type titanium alloy processed by ultrasonic nanocrystal surface modification. The USR treatment can be considered as micro-cold-forging effect on the grains [14], leading to severe dislocation of the original grains interior and boundary. It was reported that some dense dislocations can be found in the grain interior and boundaries in the ultrasonic surface rolling processing treated 40Cr steel and titanium alloy [12, 15]. Dense dislocation can provide the strain energy with high density. The new boundaries of grains can be formed by the mode of annihilating, accumulating and rearranging of dislocation [16]. With the dislocation accumulating at the grain boundaries, the dislocation density was increased.

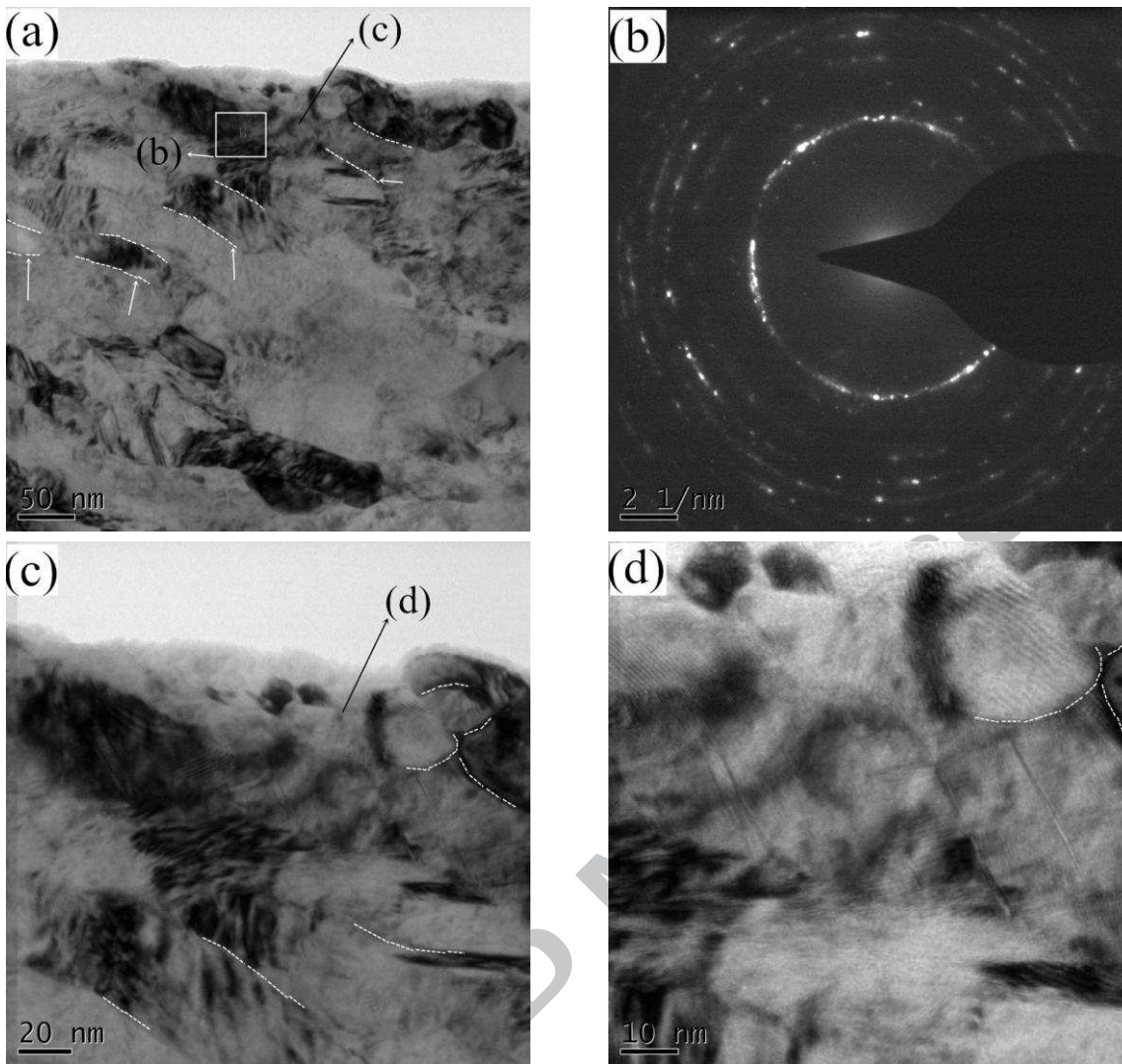


Fig. 7 TEM images from the top surface of USR treated specimen: (a) bright field image; (b) selected area electron diffraction pattern; (c),(d) enlarged bright field image.

3.2 Residual stress, surface roughness and microhardness profile

The surface roughness (R_a , arithmetical mean deviation of the profile) values after the USR treatment in the surface zone are presented in Fig. 8, and the compressive residual stress distribution of different specimens is presented in Fig. 9. The average surface roughness of the untreated material was $0.84 \mu\text{m}$, and the average surface roughness of the treated material was decreased to $0.25 \mu\text{m}$ and $0.21 \mu\text{m}$. It is observed that the untreated specimen had a -210 MPa residual stress, which resulted from the machining process of the specimens.

After the USR treatment at 20 kHz and 900 N, the treated specimen had an average residual stress of -751 MPa on the surface and -808 MPa at a depth of $20\ \mu\text{m}$ and -831 MPa at $50\ \mu\text{m}$. For the treated specimens at 30 kHz and 900 N, the residual stress reached -803 MPa on the surface and -876 MPa at a depth of $20\ \mu\text{m}$ and -908 MPa at $50\ \mu\text{m}$. Compared to the USR treatment at 20 kHz, it was found that a higher residual stress and lower surface roughness could be produced through the treatment at a frequency of 30 kHz. It can be attributed to a higher grain dislocation being produced by a vibration with higher frequency, which means a higher energy. However, as reported by Qu et al. [15], the USR treatment at 40 kHz lead to slight oxidation and adhesion behaviour on the surface of Ti-6Al-4V titanium material due to the excessive transient impact energy. Based on the comparative results and former researches [15-17], the USR treatment at 30 kHz at 900 N was considered to be a suitable processing parameter for 23-8N engine valve steel. The different depth and residual stress were obtained from different severe plastic deformation processes. It was reported in many studies that different severe plastic deformation surface treatments would lead to different distributions and depth of compressive residual stress [12, 23-25].

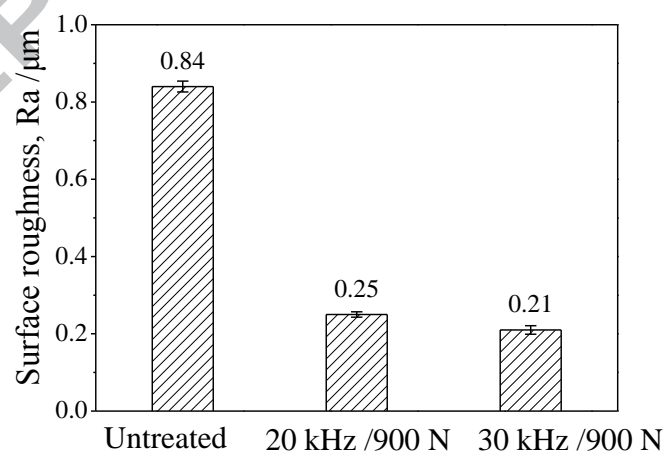


Fig. 8 Surface roughness Ra of different specimens.

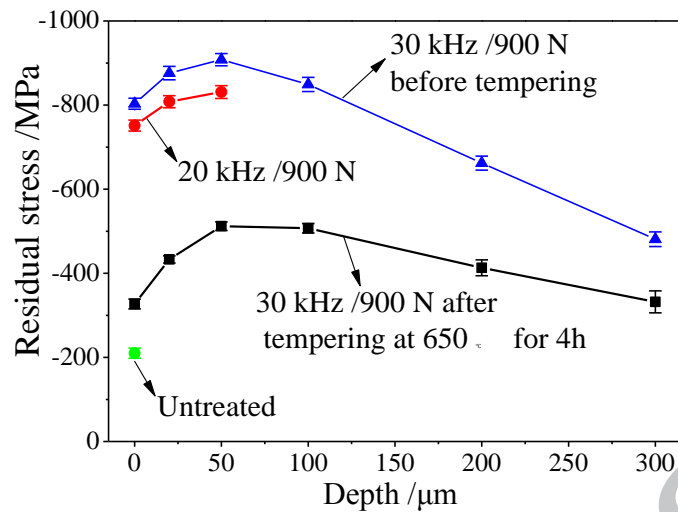


Fig. 9 Comparison of residual stress variation with depth.

Fig. 10 presents the microhardness profile of the cross-sectional surfaces. The hardened depth after USR treatment at 20 kHz and 30 kHz was 710 μm and 800 μm, respectively. As reported by Wu et al., the hardened depth value of plasma-nitrided S45C steel after ultrasonic nanocrystal surface modification treatment was about 800 to 1000 μm [10]. However, the hardened depth of Ti-6Al-4V titanium material was only about 20 μm to 60 μm [15-17]. According to the Hall-Petch relationship [26], the microhardness of the material surface and severe plastic deformation layer could be increased by good grain refinement, and the work hardening effect will be produced by plastic compressive deformation, which resulted from the high frequency ultrasonic surface impacts. Based on the compressive residual stress distribution (Fig. 9) and microhardness profile of the cross-sectional surfaces (Fig. 10) of USR treated specimen, it can be derived that a higher value of residual stress accompanied by a higher microhardness.

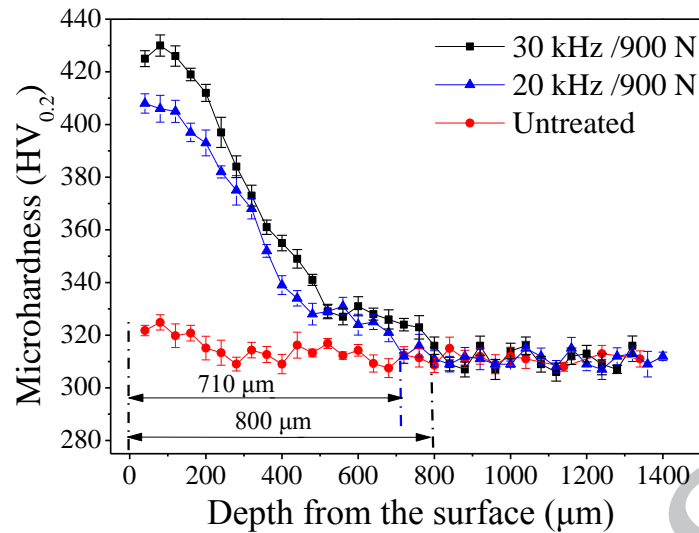


Fig. 10 Microhardness profile of cross-sectional surface.

3.3 Fretting wear behaviour

3.3.1 Coefficient of friction

The coefficient of friction (CoF) for the different material conditions are presented in Fig. 11(a). Compared to the untreated materials, the CoF of the USR treated material is significantly decreased. It has also been reported by other researchers that surface modified layers generated by severe plastic deformation processes could lead to a reduction in CoF [15, 23, 27]. Furthermore, the frequency of ultrasonic vibration has an evident effect on the value of the CoF curve. The CoF of material treated at 30 kHz was lower than that treated at 20 kHz. Fig. 11(b) presents the CoF of the treated (30 kHz, 900 N) material under different fretting loads. With an increase of fretting load from 5 N to 40 N, the CoF further decreased. It can also be seen that more serious fluctuation of CoF occurred in the steady-state period of the tests with high fretting load (40 N).

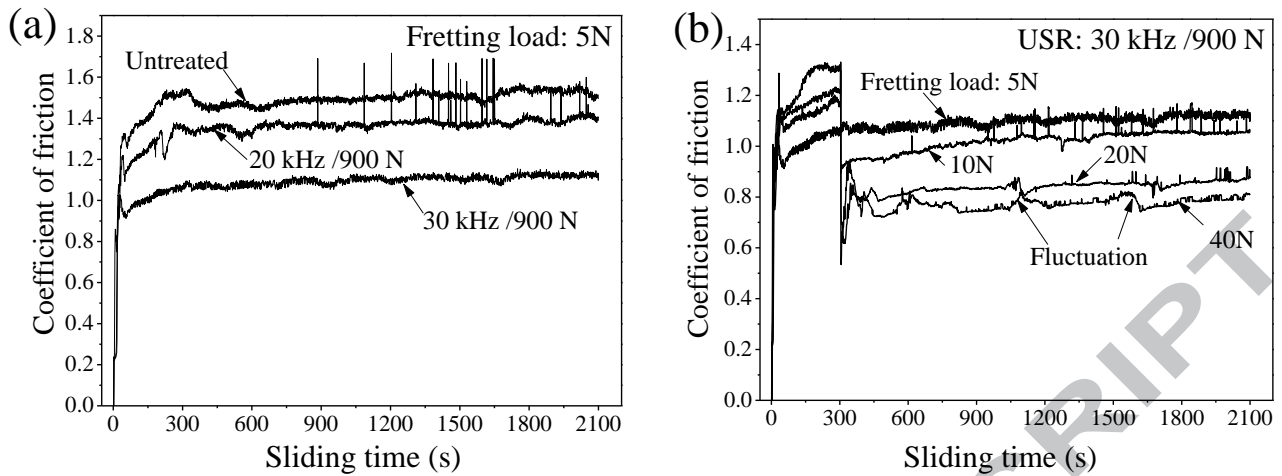


Fig. 11. (a) The CoF of the different materials; (b) the CoF of USR treated (30 kHz, 900 N)

materials with different fretting loads.

3.3.2 Wear resistance and wear mechanisms

After the fretting wear tests, the worn surfaces of the specimens were evaluated by SEM. The results of wear scar area are presented in Fig. 12, and the SEM images of fretting wear tracks and the corresponding EDS results are presented in Fig. 13. Compared to the virgin material, the wear resistance of the treated materials was significantly increased (Fig. 12). The wear scar area was decreased 11.3 % (from 1.33 mm² to 1.18 mm²). This result can be attributed to the higher hardness and increased level of compressive residual stress of the modified surface layers, which resulted from the refinement of the grain size and the internal strain of the crystal lattice introduced by the USR treatment. Furthermore, the wear resistance of the material treated at 30 kHz was better than that treated at 20 kHz, indicating that a higher frequency of ultrasonic vibration can produce a higher hardness and compressive residual stress (Fig. 9), and likely a better wear resistance. With the increase of fretting loads, the wear scar area was increased.

In addition, the effective improvement in the wear resistance of the austenitic engine valve steel makes it possible that USR treatment could be also utilized for the stem of a poppet engine valve.

During the engine operation, wear problems can occur in the valve stem-guide contact, because of the high frequency reciprocating relative sliding motion of valve stem and valve guide, therefore excellent wear resistance is required [1]. Typically, engine valve stem surfaces are enhanced by chromium plate or nitriding treatment [28] but there is a need however to develop new technologies, avoiding environmental issues during the chromium plate processing. Based on the current results, the USR treatment is a potential solution for a valve stem to be more wear resistant.

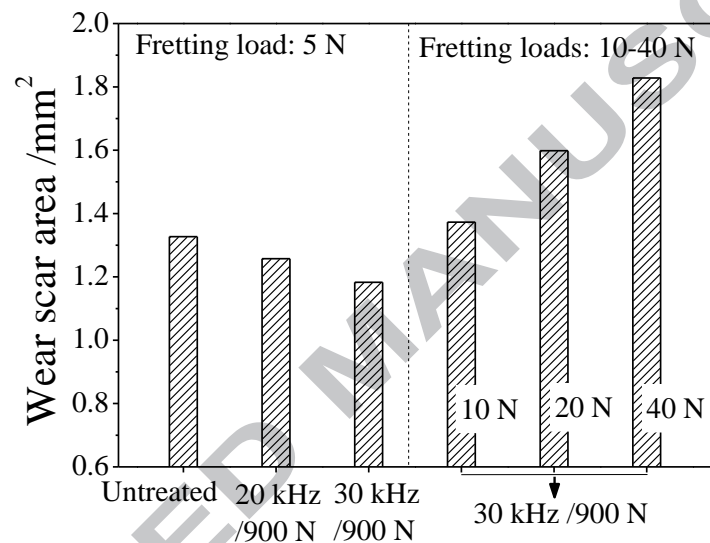


Fig. 12. Wear scar area of untreated and treated specimens.

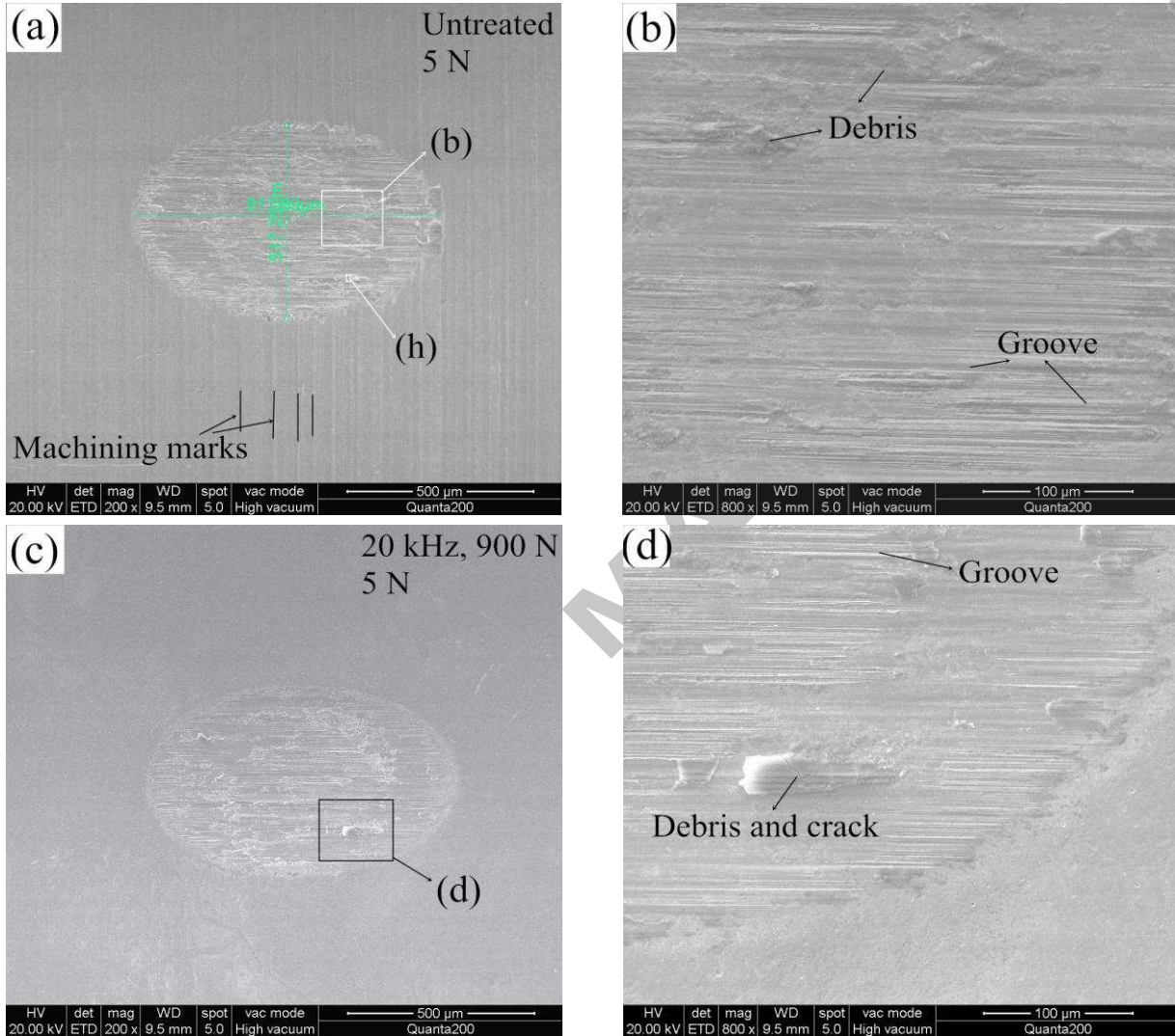
The machining marks (labeled in black lines in Fig. 13(a).) could be observed in the non-contact area on the untreated material surface. However, the non-contact areas on the surface of the treated materials are seen to be much smoother with a lower surface roughness (Fig. 13(c) and (e)), which has been also verified in Section 3.2 (Fig. 8). It is believed that wear debris particles would be generated from the relative movement of contact surfaces under pressure. Many of the debris particles would be removed from the rubbing interface due to the reciprocating sliding with fretting loads, leading to the wear loss of materials, but other debris particles are retained between the rubbing surfaces. These debris persist and agglomerate in the contact zones as moving particles

ploughed the surfaces to generate grooves. Consequently, slight grooves are characterized in the worn areas of all materials, as presented in Fig. 13(b), (d), (f) and (g). The generation of these grooves and slip regions can be identified as abrasive wear during sliding [17].

As sliding continues, some of the debris particles (already agglomerated or individually) retained in the contact were highly compacted together to form localized tribolayers covering a part of the worn surfaces. The agglomeration behaviour of debris from the three specimen types were different. As presented in Fig. 13(b), the tribological layers on the untreated material were seen to be more consolidated than those on the treated materials, which could be attributed to the debris with lower hardness spalled from the untreated materials being easier to compact in the contact. These exhibit a better relative wear resistance, because of a higher hardness and compressive residual stress of surface and subsurface of the treated materials, as indicated in Fig.12. It is believed that micro-scale debris from the treated materials still maintains finer grains and higher hardness. Thus, such debris is more difficult to compact to form the localized tribolayers. Under the pressing and sliding of the counterface (the ceramic ball), the layers were delaminated. Those broken layers and debris agglomerated together near the edge of the worn area, as illustrated in Fig. 13(d), (f) and (g). Thus, the wear mechanisms of USR treated material are also identified as adhesion and delamination.

The remaining debris and formed layers were further ground, rolled and compacted. Compared to the EDS results of the non-contact area of material (Fig. 13(i)), oxygen and silicon element percentage was increased in the worn areas of the untreated and treated materials (Fig. 13(h) and (j)), as well the aluminium element was detected in these worn areas. Aluminium and silicon were transferred from the (ceramic ball) counterface to the steel worn surfaces. It is indicated that a certain wear existed on the surface of ball, even though the Si_3N_4 ceramic material has a much

higher hardness of 1500 HV_{0.5} [17, 29]. Additionally, the increase of oxygen present on the worn surfaces of the untreated and treated materials can be considered evidence of the existence of oxidative wear.



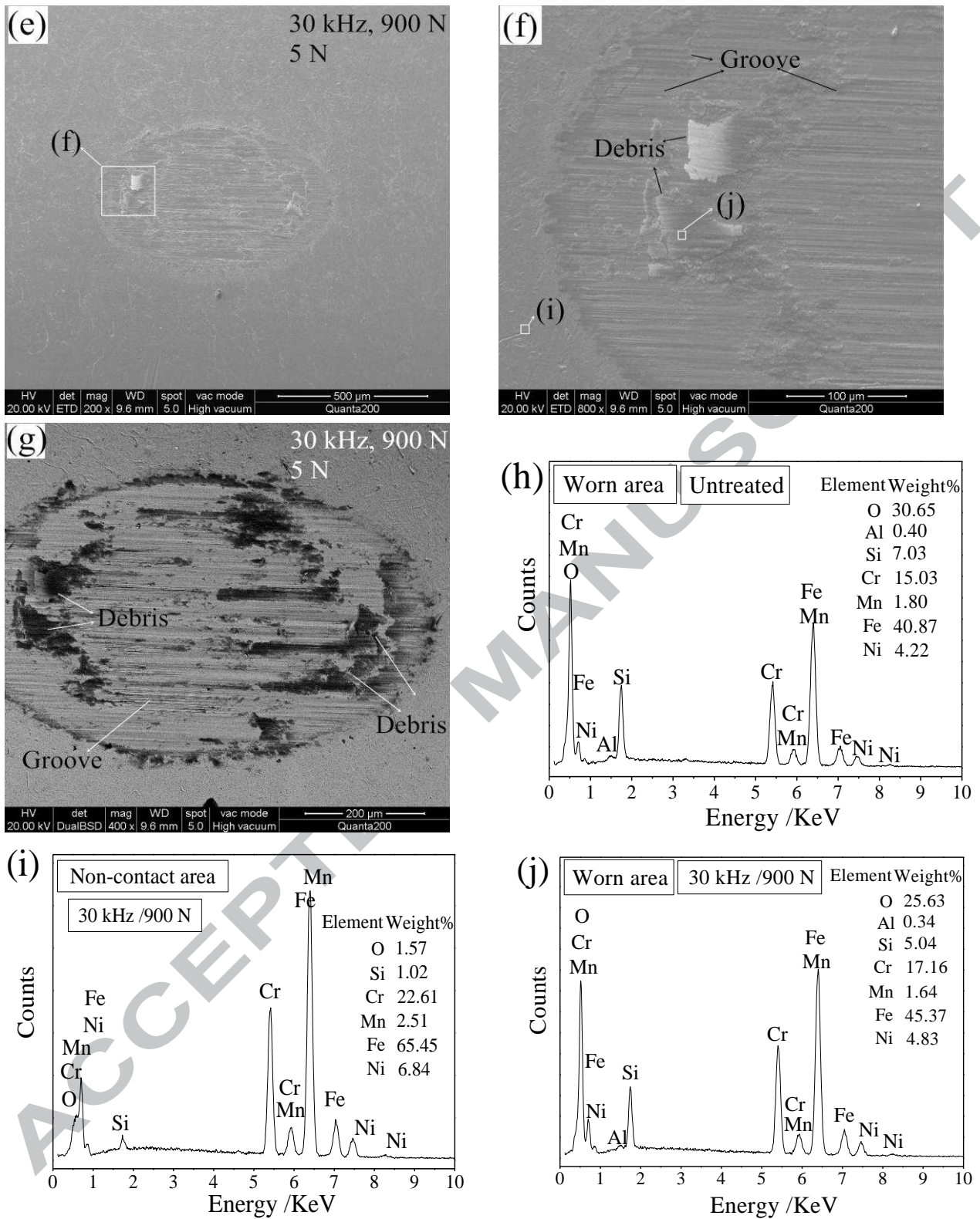


Fig. 13 (a-g) Worn surfaces of the specimens after fretting wear test; (h-j) the EDS results of worn surfaces.

3.4 Fatigue behaviour

3.4.1 Fatigue results and S-N curves

Based on the results of microhardness, compressive residual stress and fretting wear test (Sections 3.2 and 3.3), the USR treatment at 30 kHz at 900 N is considered to obtain the best performing modified layer. Hence, the specimens for the rotating bending fatigue test were processed through treatment at 30 kHz at 900 N. The fatigue results of specimens with and without treatment at the two temperatures were statistically analysed and the S–N curves are illustrated in Fig. 14. Then, according to the S–N equation and curve, the fatigue strength on the base of 10 million cycles can be determined. Compared to the untreated specimens, the fatigue strength of the specimens at 25 °C after treatment increased 38.3 % (from 528 MPa to 730 MPa). At 650 °C, the fatigue strength increased 15.9 % (from 345 MPa to 400 MPa). The results show that USR treatment would produce a significant extension in fatigue resistance.

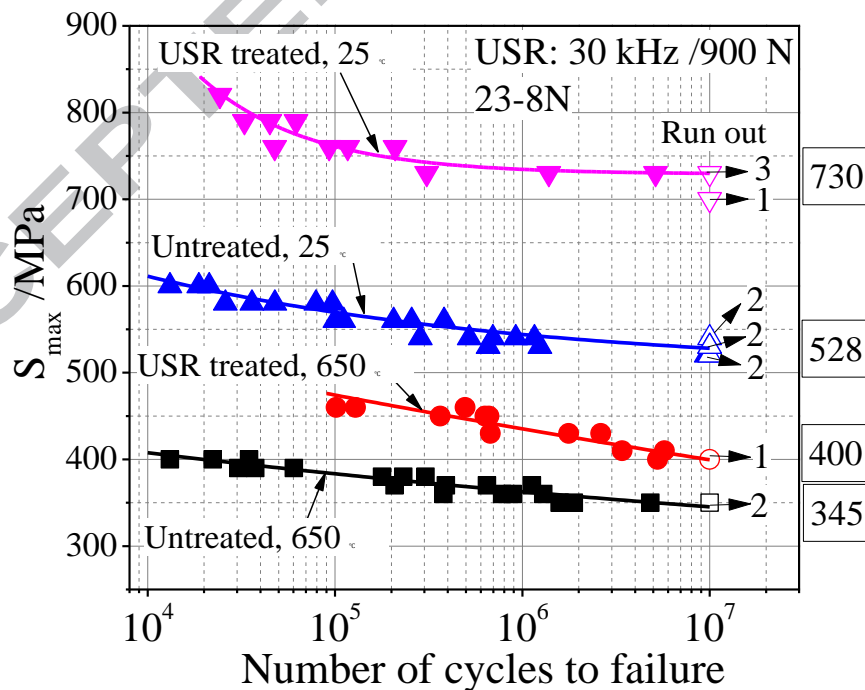
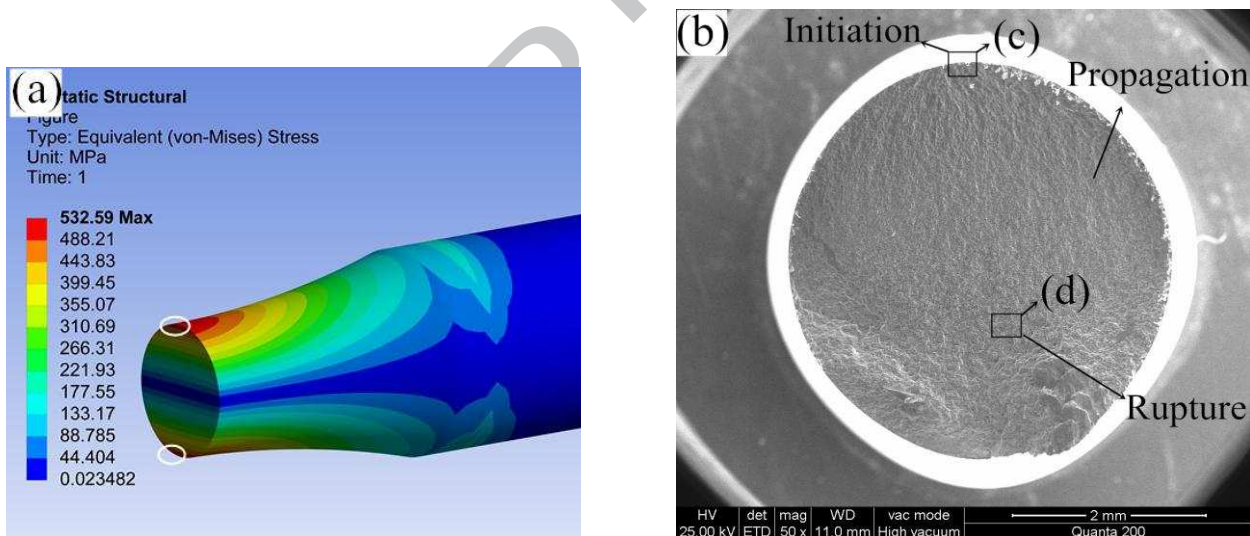


Fig. 14. S-N curves of rotating bending fatigue tests at 25 °C and 650 °C.

3.4.2 Fracture surface and mechanisms

The fractured surfaces of the hourglass shape fatigue specimens were cleaned and then observed by SEM. Fig. 15(a) shows the von Mises stress of the specimen at a nominal bending stress (produced by weight and lever in the tester) of 530 MPa, it is found that the maximum von Mises stress occurs on the surface of the round notch of the specimen, as indicated by the white circles. As presented in Fig. 15(b), three clear regions existed in the typical fracture surfaces of the untreated specimens, including the crack initiation region, the crack propagation region and the final rupture region. During the fatigue test, the cracks initiated on the surface of specimen (Fig. 15(c)). After the initiation of cracks, cracks displayed as fluvial stripes in the crack propagation region. Finally, the specimen would fracture. Fig. 15(d) presents the fatigue final rupture region, which is significantly more precipitous than the other two regions.



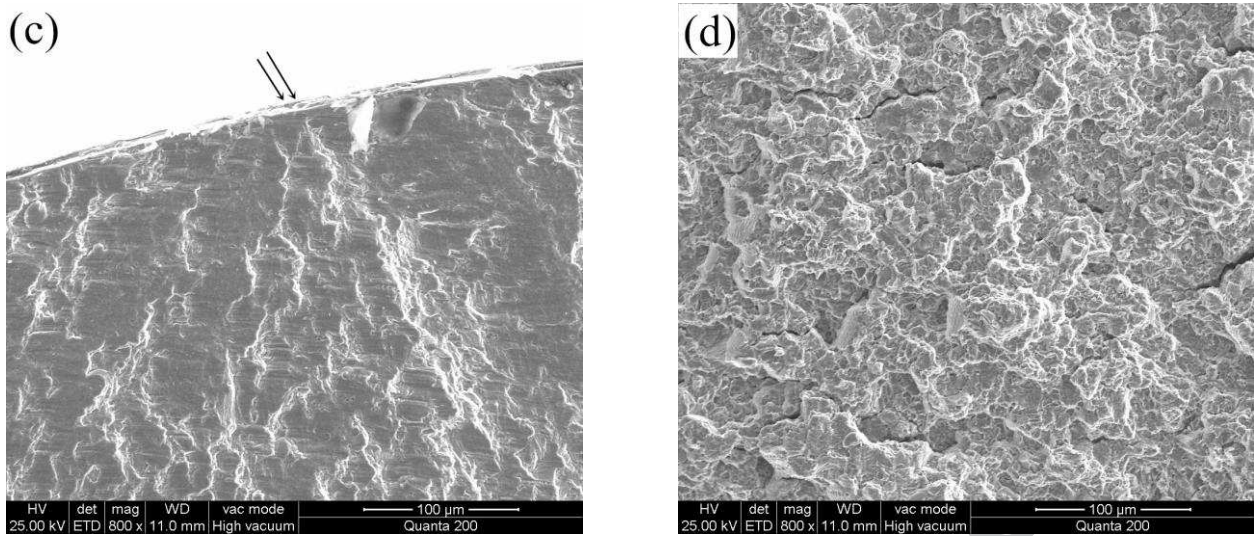


Fig. 15 (a) The von Mises stress of untreated specimen at the bending stress of 530 MPa at 25 °C;

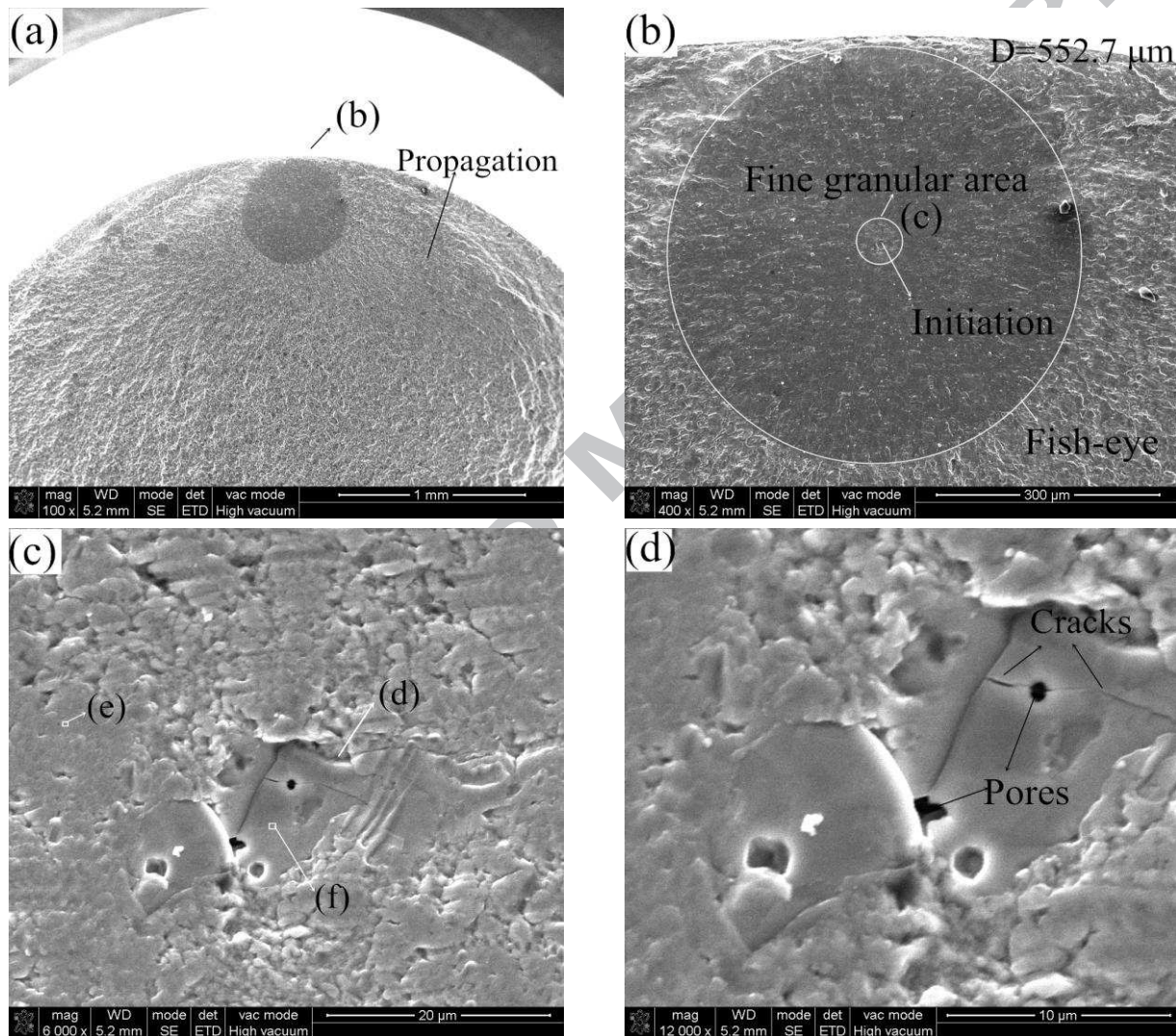
(b-d) typical fracture surfaces of the untreated specimen tested at 25 °C ($S_{\max} = 540$ MPa, $N = 285,503$ cycles).

For the fracture surfaces of treated specimens tested at lower loads at 25 °C, the crack initiation sites are shifted to the subsurface region (Fig. 16(a) and (b)), leading to the forming of a fish-eye pattern. It can be seen from the Fig. 16(c) and (d) that the fatigue cracks initiated from an internal inclusion in the specimen, and the internal inclusion was always located at the centres of the fish-eye. In the vicinity of the inclusion, one area often described as a fine granular area was observed [30], as indicated by the smaller white circle in Fig. 16(b). It is also reported by Qu et al. and Suh et al. that the crack initiation position was shifted to the subsurface region after the surface enhancement with ultrasonic vibration technology [16, 23]. As presented in Fig. 9, compared to the untreated specimen, the USR treatment produces much higher compressive residual stress on the specimen surface and subsurface, the maximum residual stress reached -908 MPa at a depth of 50 μm. Zhu et al. reported that the crack initiation process is affected by the gradient distribution of residual stress from specimen surface to matrix material [31]. For the USR treated specimen, it is inferred that the produced residual stress could change the actual applied mean stress leading to a

location dependent strength along the specimen cross section [31]. The cracks initiated in the subsurface region of specimens which were tested at lower loads. However, the residual stress were relaxed during cyclic loading in the fatigue test [32]. Additionally, the residual stress would relax in the initial cycles in the fatigue test, and a higher fatigue load would lead to a faster residual relaxation at room temperature [31]. This agrees well with the fact that the cracks also initiated on the surface of treated specimen tested at higher loads.

Fig. 16(e) and (f) present the EDS results of the matrix material and the inclusion in the fine granular area, respectively. Compared to the matrix material, much higher carbon and chromium weight percentage were detected in the inclusion, indicating likely brittleness of the inclusion. Sakai et al. investigated the fatigue properties of a bearing steel in the long-life region. They concluded that the fatigue fracture of the bearing steel in the long-life region contained three processes: the formation of a fine granular area, crack propagation to form the fish-eye and rapid crack propagation to cause fracture [30]. In the research on the inclusion-induced interior cracking mechanisms, Zhu et al. conducted a study of a precipitation-hardened stainless steel in high cycle and very high cycle fatigue regimes [33]. They found that the physics of inclusion-induced interior cracking is a microstructure-dependent crack initiation and stage I growth process. Similarly, small cracks and pores were observed in the inclusion (Fig. 16(c) and (d)). Furthermore, after the martensitic laths's breakdown, dislocation cell structures were formed in the stainless steel, and the fine granular area on the fracture surface was characteristic of several nano-scale grains [33]. In addition, in the investigation of failure mechanisms and fatigue assessment of a low strength steel welded joint, Zhu and Xuan proposed a physical criterion for formation of a fine granular area: the ratio of accumulation to release rates of cyclic plastic energy was higher than one [34]. In the

current research, the fish-eye pattern and fine granular area were only observed in two USR treated specimens whose fatigue life was more than one million cycles at 25 °C. They were tested at relative lower applied load with a longer fatigue life. It could be concluded that the USR treatment influenced the fracture mechanism and the formation of a fine granular area, leading to shift of the crack initiation sites from the surface to the subsurface region.



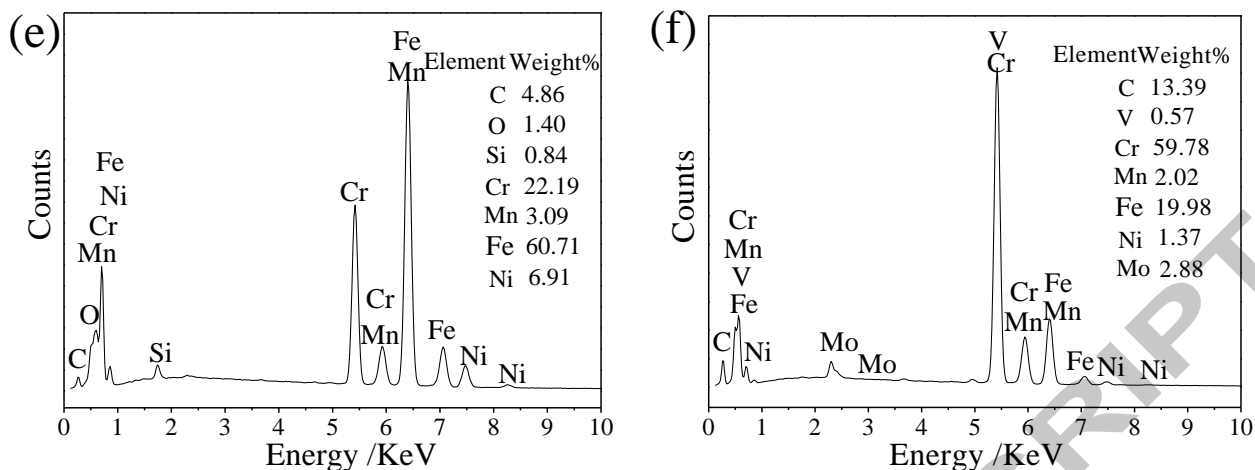


Fig. 16 (a-d) Fracture surfaces of the USR treated specimen tested at 25 °C; (e-f) EDS results of the inclusion area on specimen surfaces ($S_{\max} = 730$ MPa, $N = 5,145,187$ cycles).

Fracture surfaces of the untreated specimen tested at 650 °C are presented in Fig. 17, and the fracture surfaces of the USR treated specimen are presented in Fig. 18. Generally, it is found that the typical fracture surfaces can be classified as three regions, as presented in Fig. 17(a), which is similar to Fig. 15(b). The cracks initiated on the surface of the specimen (Fig. 17(b)), which is similar to Fig. 15(c). For a USR treated specimen tested at 410 MPa, the cracks were observed in the region very close to the surface (Fig. 18(b)), indicating the crack initiation sites was shifted to the subsurface region. However, compared to the USR treated specimen tested at 25 °C, the shift distance was much smaller and no fish-eye pattern and a fine granular area were formed on the fracture surface. Fig. 9 presents the residual stress distribution of the USR treated (30 kHz, 900 N) specimens before and after tempering at 650 °C for 4 h. It could be noted that residual stress relaxation occurred at high temperature. After heating at 650 °C, the compressive residual stress on specimen surface was relaxed from -803 MPa to -329 MPa. The maximum residual stress still existed at a depth of 50 μm , and it was relaxed from -908 MPa to -512 MPa. It is also reported by Zhu et al. that more serious degradation of residual stress (even under lower applied loads) occurred at

higher temperatures [31]. Furthermore, the applied fatigue load and the number of fatigue cycles resulted in the relaxation of residual stress. It could be ascribed to the combination of thermally activated processes and cyclic deformation during the test [31]. Hence, the decrease of the shift distance of crack initiation sites from the surface to subsurface at high temperatures can be attributed to the material performance degradation of severe plastic deformation layer, including the softening and oxidation of the material and relaxation of the compressive residual stress.

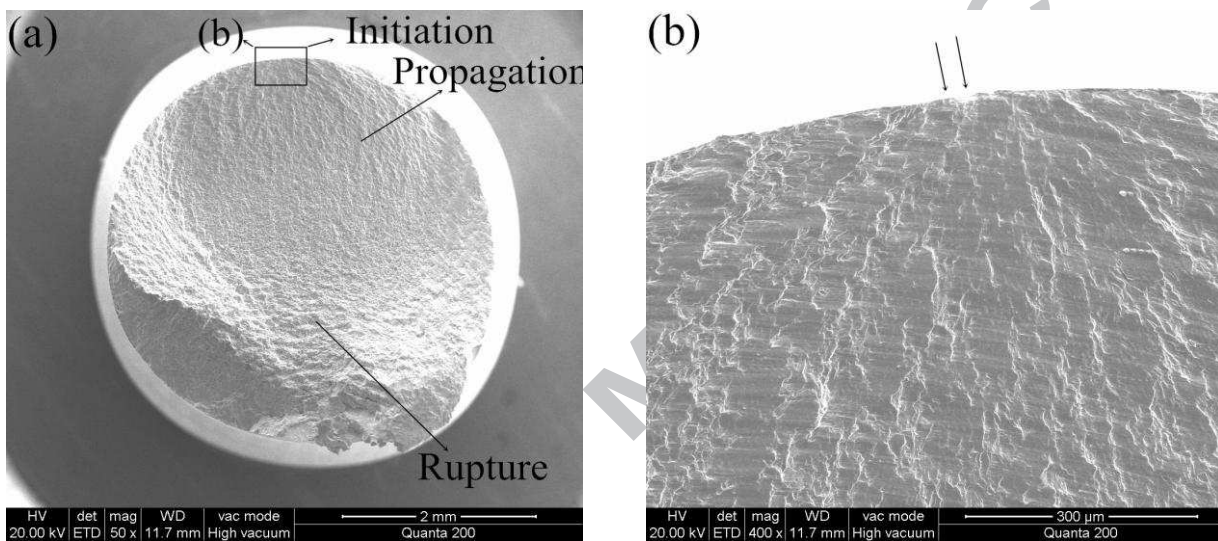


Fig. 17 (a), (b) Fracture surfaces of the untreated specimen tested at 650 °C ($S_{\max} = 370$ MPa, $N = 647,502$ cycles).

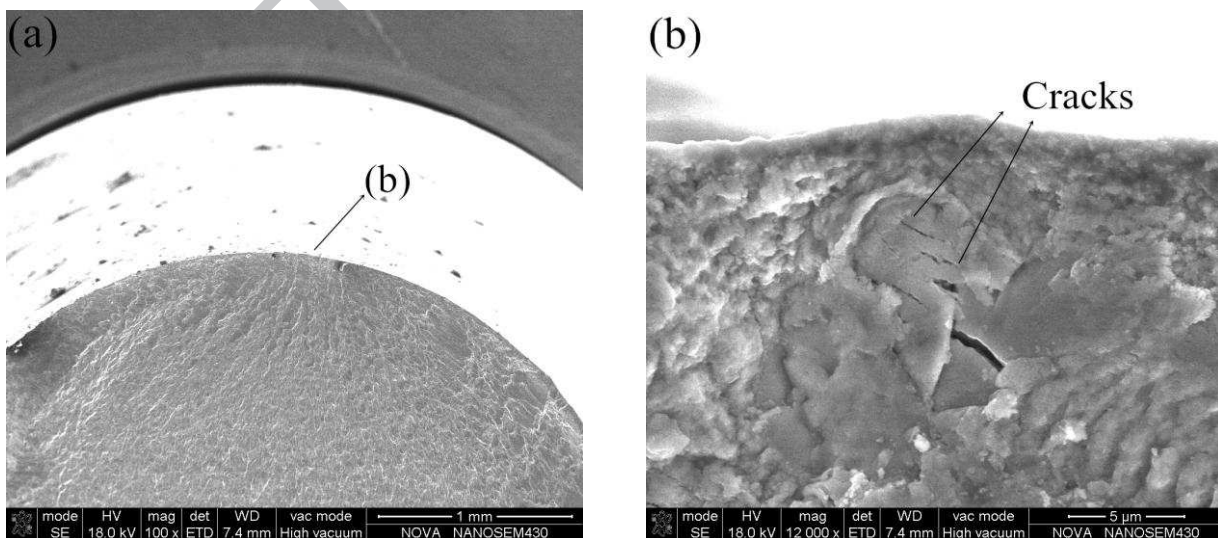


Fig. 18 (a), (b) Fracture surfaces of the USR treated specimen tested at 650 °C ($S_{\max} = 410$ MPa,

N=5,732,637 cycles).

According to the results obtained from fracture surface of specimens and the results reported by Lu et al. [35], the fatigue fracture mode was classified into two types: surface and subsurface fracture mode. It is found that the surface fracture mode is predominant at high stress levels in the two materials. At low stress levels, the surface fracture mode is predominant for the untreated specimens, but the subsurface fracture mode is the main failure mode of the treated specimen, especially for the specimens with fatigue life that was more than 10^6 cycles. From the fracture mechanics viewpoint, the inclusions in the high-strength steels are the initial defects [35]. It was also reported by Nishijima and Kanazama that an internal failure mode is especially important for fatigue life in the gigacycle range, as this mode is predominant at low stress ranges [36]. However, Shiozawa et al. reported that the inclusion would develop a fish-eye fracture mode (internal failure mode) that was distributed over a wide range of stress amplitude [37]. The subsurface fracture mode not only occurred when the applied stress level was below the fatigue limit of material, but also when the stress level was above the fatigue limit [37].

With the introduction of severe plastic deformation layers on the surface of specimen through the USR treatment, the possible subsurface cracks caused by machining can be restrained. Due to the crack branching and deflection in the more randomly oriented microstructures of severe plastic deformation layer, the crack propagation rate was reduced [38]. Indeed, the more randomly oriented microstructures with nanoscale were also verified in the results earlier presented in Fig. 5 and Fig. 7. Consequently, it can be concluded that the extension of fatigue resistance of USR treated specimen can be attributed to a combination of beneficial compressive residual stress, work hardening, and the modified microstructure with fine-grains in the severe plastic deformation layer.

4. Conclusions

Ultrasonic surface rolling technology was introduced to a 23-8N engine valve steel. The wear resistance and fatigue strength were significantly improved. Some conclusions can be drawn as follows:

- (1) The microstructure of the top surface of ultrasonic surface rolling treated material consisted of lamellar grains with nanoscale, and the width of the grains was about 50–150 nm. The lamellar grains consisted of nanostructured subgrains with a non-uniform morphology.
- (2) The ultrasonic surface rolling treatment introduces a higher compressive residual stress and lower surface roughness of the material surface. The frequency of 30 kHz of ultrasonic vibration could produce a higher compressive residual stress and lower surface roughness than that produced by the frequency of 20 kHz.
- (3) The surface modified layers generated by the ultrasonic surface rolling treatment leads to a reduction in coefficient of friction, and the wear resistance was increased.
- (4) The fatigue strength of 23-8N engine valve steel specimen was improved by ultrasonic surface rolling treatment from 528 MPa to 730 MPa at 25 °C; from 345 MPa to 400 MPa at 650 °C. The ultrasonic surface rolling treatment is a potential solution for engine valve to improve fatigue resistance.
- (5) The improvement of fatigue resistance and wear resistance of a ultrasonic surface rolling treated specimen can be attributed to a combination of beneficial compressive residual stress, work hardening, and the modified microstructure with fine-grains in the severe plastic deformation layer.

Acknowledgements

Here we wish to express the most heartfelt appreciation to Chairman Tao Zhang from Huaiji Dengyun Auto-parts (Holding) Co., LTD. The authors acknowledge Senior Engineer Huahuan Luo, Dongqiang Mo, Gang Chen and Engineer Ge Sun from Huaiji Dengyun Auto-parts (Holding) CO., LTD. for providing the professional guidance and help for the paper. We are thankful for the financial support from the Guangdong Province Scientific and Technological Projects (No. 2016KZ010104) and from the China Scholarship Council (File No. 201706150079). The work was also sponsored by the open fund project of State Key Laboratory of Engine Reliability (SKLER-201705).

Conflicts of Interest: The authors declare no conflict of interest.

References

- [1] YS Wang. Introduction to engine valvetrains. Warrendale: SAE International; 2007.
- [2] SB Caird, DM Trela. High temperature corrosion-fatigue test method for exhaust valve alloys. SAE 810033, 1980.
- [3] FQ Lai, SG Qu, Y Duan, et al. The wear and fatigue behaviours of hollow head & sodium filled engine valve. Tri. Int. 2018; 128:75–88.
- [4] RP Worthen, DG Rau. Measurement of valve temperatures and strain in a firing engine. SAE 860356, 1986.
- [5] DR Jones. Fatigue behaviour of exhaust valve alloys. SAE 800315, 1980.
- [6] PM Lerman, RPF Almeida. Heavy duty valves with enhanced performance through nitriding

treatment. SAE 2015-36-0240, 2015.

- [7] M Larson, A Melander, R Blom, S Preston. Effects of shot peening on bending fatigue strength of spring steel SS 2090. *Materials Science and Technology*, 1991;7: 998-1004.
- [8] KA Soady, BG Mellor, et al. Evaluating surface deformation and near surface strain hardening resulting from shot peening a tempered martensitic steel and application to low cycle fatigue. *Int J Fatigue* 2013; 54:106–117.
- [9] PK Nalla, I Altenberger, et al. On the influence of mechanical surface treatments—deep rolling and laser shock peening—on the fatigue behavior of Ti-6Al-4V at ambient and elevated temperatures. *Mat Sci Eng A-Struct* 2003; 355: 216–230.
- [10] B Wu, P Wang, et al. Effect of ultrasonic nanocrystal surface modification on the fatigue behaviors of plasma-nitrided S45C steel. *Surf Coat Tech* 2012; 213:271–277.
- [11] B Wu, J Zhang, et al. Effect of ultrasonic nanocrystal surface modification on surface and fatigue properties of quenching and tempering S45C steel. *Appl Surf Sci* 2014;321:318–330.
- [12] T Wang, DP Wang, G Liu, BM Gong, NX Song. Investigations on the nanocrystallization of 40Cr using ultrasonic surface rolling processing. *Appl Surf Sci* 2008;255:1824–1829.
- [13] A Amanov, R Umarov. The effects of ultrasonic nanocrystal surface modification temperature on the mechanical properties and fretting wear resistance of Inconel 690 alloy. *Appl Surf Sci* 2018;441:515–529.
- [14] S Chang, YS Pyun, A Amanov. Wear enhancement of wheel-rail interaction by ultrasonic nanocrystalline surface modification technique. *Materials* 2017; 188(10): 1–12.
- [15] G Li, SG Qu, YX Pan, XQ Li. Effects of the different frequencies and loads of ultrasonic surface rolling on surface mechanical properties and fretting wear resistance of HIP Ti-6Al-4V

alloy. *Appl Surf Sci* 2016;389:324–334.

- [16] G Li, SG Qu, MX Xie, et al. Effect of multi-pass ultrasonic surface rolling on the mechanical and fatigue properties of HIP Ti-6Al-4V Alloy. *Materials* 2017; 133(10): 1–15.
- [17] G Li, SG Qu, MX Xie, XQ Li. Effect of ultrasonic surface rolling at low temperatures on surface layer microstructure and properties of HIP Ti-6Al-4V alloy. *Surf Coat Tech* 2017; 316:75–84.
- [18] JM Gere, SP Timoshenko. *Mechanics of Materials*, 4th ed. PWS Publishing Company. Boston, MA, USA; 1997.
- [19] L Saraf. Kernel Average Misorientation confidence index correlation from FIB sliced NiFe-Cr alloy surface. *Microsc Microanal* 2011; 17 (Suppl 2): 424–425.
- [20] HL Li, E Hsu, J Szpunar, et al. Deformation mechanism and texture and microstructure evolution during high-speed rolling of AZ31B Mg sheets. *J Mater Sci* 2008; 43:7148–7156.
- [21] V Randle, O Engler. *Introduction to texture analysis macrotexture, microtexture and orientation mapping*. Boca Raton, CRC PRESS, 2000.
- [22] M Kheradmandfard, SF Kashani-Bozorg, CL Kim, et al. Nanostructured β -type titanium alloy fabricated by ultrasonic nanocrystal surface modification. *Ultrason Sonochem* 2017; 39: 698–706.
- [23] CM Suh, GH Song, MS Suh, YS Pvoun. Fatigue and mechanical characteristics of nano-structured tool steel by ultrasonic cold forging technology. *Mat Sci Eng A-Struct* 2007; 443: 101–106.
- [24] S Bagherifard, M Guagliano. Fatigue behavior of a low-alloy steel with nanostructure surface obtained by severe shoe peening. *Eng Fract Mech* 2012;81:56–68.

- [25] K Dai, L Shaw. Comparison between shot peening and surface nanocrystallization and hardening processes. *Mat Sci Eng A-Struct* 2007;463:46–53.
- [26] NA Prakash, R Gnanamoorthy, M Kamaraj. Microstructural evolution and mechanical properties of oil jet peened aluminium alloy, AA6063-T6. *Mater Design* 2010;31:4066–4075.
- [27] A Amanov, IS Cho, DE Kim, YS Pyun. Fretting wear and friction reduction of CP titanium and Ti-6Al-4V alloy by ultrasonic nanocrystalline surface modification. *Surf Coat Tech* 2012; 207:135–142.
- [28] PM Lerman, RP Almeida. Heavy duty valves with enhanced performance through nitriding treatment. SAE 2015-36-0240, 2015.
- [29] A Kumar, S Ghosh, S Aravindan. Grinding performance improvement of silicon nitride ceramics by utilizing nanofluids. *Ceram Int* 2017;43: 13411–13421.
- [30] T Sakai, Y Sato, N Oguma, Characteristic S-N properties of high-carbon-chromium-bearing steel under axial loading in long-life fatigue. *Fatigue Fract Engng Mater Struct* 2010; 25: 765-773.
- [31] ML Zhu, FZ Xuan, YN Du, ST Tu. Very high cycle fatigue behavior of a low strength welded joint at moderate temperature. *Int J Fatigue* 2012; 40:74–83.
- [32] CR Sohar, A Betzwar-Katas, C Gierl, B Weiss, H Danninger. Gigacycle fatigue behavior of a high chromium alloyed cold work tool steel. *Int J Fatigue* 2008; 30:1137–1149.
- [33] ML Zhu, J Long, FZ Xuan. Fatigue life and mechanistic modeling of interior micro-defect induced cracking in high cycle and very high cycle regimes. *Acta Mater* 2018;157:259–275.
- [34] ML Zhu, FZ Xuan. Failure mechanisms and fatigue strength assessment of a low strength Cr-Ni-Mo-V steel welded joint: Coupled frequency and size effects. *Mech Mater*

2016;100:198–208.

- [35] LT Lu, JW Zhang, K Shiozawa. Influence of inclusion on S-N curve characters of high-strength steels in the giga-cycle fatigue regime. *Fatigue Fract Eng M* 2009; 32: 647–655.
- [36] S Nishijima, K Kanazama. Stepwise S-N curve and fish-eye failure in gigacycle fatigue. *Fatigue Fract Engng Mater Struct* 1999;22: 601–607.
- [37] K Shiozawa, L Lu, S Ishihara. S–N curve characteristics and subsurface crack initiation behaviour in ultra-long life fatigue of a high carbon-chromium bearing steel. *Fatigue Fract Engng Mater Struct* 2001;24: 781–790.
- [38] A Vinogradov. Fatigue limit and crack growth in ultra-fine grain metals produced by severe plastic deformation. *J Mater Sci* 2007; 42:1797–1808.

Highlights

- (1) 23-8N engine valve steel was treated by ultrasonic surface rolling technique.
- (2) The microstructures of the modified layer were nano-scale lamellar grains.
- (3) The treatment led to a reduction in surface roughness and coefficient of friction.
- (4) The fatigue strength and wear resistance were increased after treatment.
- (5) The cracks initiation mechanism was influenced by the residual stress in specimens.